JOC Note
pubs.acs.org/joc

# Bingel−Hirsch Reactions on Non-IPR $Gd_3N@C_{2n}$ ($2n$ = 82 and 84)

Núria Alegret,[†] Manuel N. Chaur,[‡] Eva Santos,[†] Antonio Rodríguez-Fortea,[†] Luis Echegoyen,*[,‡] and Josep M. Poblet*[,†]

[†]*Departament de Química Física i Inorgànica, Universitat Rovira i Virgili, c/Marcel·lí Domingo s/n, 43007 Tarragona, Spain, and* [‡]*Department of Chemistry, Clemson University, Clemson, South Carolina 29634, United States*

*josepmaria.poblet@urv.cat; luis@clemson.edu*

*Received August 30, 2010*

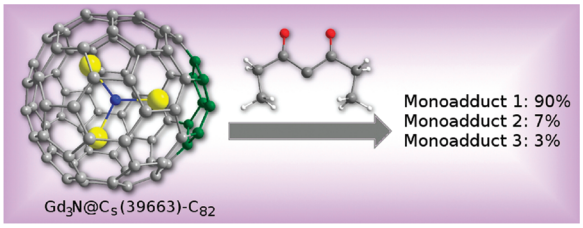


The Bingel−Hirsch reactions on non-isolated pentagon rule (non-IPR) $Gd_3N@C_{2n}$ ($2n$=82, 84) are studied. Computational results show that the two metallofullerenes display similar reactivity according to their related topologies. Long C−C bonds with large pyramidalization angles lead to the most stable adducts, the [5,6] bonds in the adjacent pentagon pair being especially favored. The lesser regioselectivity observed for $Gd_3N@C_{82}$ is probably due to the activation of some C−C bonds by means of the metal cluster.

Metallic nitride endohedral metallofullerenes (MN EMFs) have emerged as unique compounds with a wide range of potential applications.[1] Theoretically, these compounds are an interesting field of study, not only because of the electronic effect of the cluster but also for the unusual characteristics of the C−C bonds. Several calculations indicated that the thermodynamic stability of a fullerene molecule depends markedly on the negative charge that resides on it. The possibility of predicting which isomers are preferred to encapsulate MN either by checking the molecular orbital energies of the isolated carbon cages[2] or by computing the stability of the anionic cages is well established.[3]

On the other hand, derivatives of gadolinium-based MN EMFs have proven to be better contrast agents for magnetic resonance imaging (MRI) than the $Gd^{3+}$-based complexes currently in commercial use.[1,4,5] The functionalization of MN EMFs thus is a key step to take full advantage of these compounds not only for MRI applications but also for other applications such as molecular electronics and photovoltaics.[1]

**SCHEME 1. Cyclopropanation Reaction of $Gd_3N@C_{2n}$ EMFs with Diethylbromomalonate in the Presence of DBU**

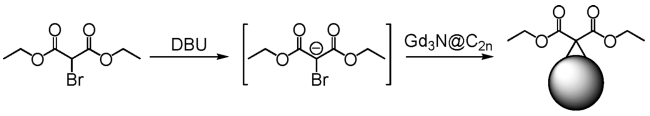


As of today, several reactions have been reported for MN EMFs of general formula $M_3N@C_{80}$.[1] In the case of larger cages, Echegoyen and co-workers reported a reactivity study of gadolinium nitride EMFs ($Gd_3N@C_{2n}$; $2n$ = 80, 84 ;and 88) toward the cyclopropanation reaction, the Bingel−Hirsch reaction (see Scheme 1).[6] The authors reported that the reactivity of the EMF is highly influenced by the fullerene size. $Gd_3N@C_{80}$ reacts readily with diethylbromomalonate in the presence of DBU to afford multiple additions if the reaction is not quenched. On the other hand, it was observed that $Gd_3N@C_{84}$ afforded only a monoadduct that was characterized by HPLC, UV−vis−NIR, MALDI-TOF MS, and electrochemistry, whereas $Gd_3N@C_{88}$ did not react at all.

Similarly to $Gd_3N@C_{84}$, only monoaddition is obtained on $Gd_3N@C_{82}$ when reacted with diethylbromomalonate under the same conditions. No signs of further additions to the fullerene cage were observed from the mass spectrum of the reaction mixture after 20 min of reaction (Figure 1). The reaction mixture was subjected to purification by HPLC using a multistage separation with a Buckyprep-M and Buckyprep columns, and three monoadducts with relative amounts 90%, 7%, and 3%, as calculated from the HPLC trace, were isolated (see Supporting Information, SI).

X-ray diffraction studies have shown that $Gd_3N$ is encapsulated, among others, in the egg-shaped non-isolated pentagon rule (non-IPR) $C_s$(39663)-$C_{82}$ and $C_s$(51365)-$C_{84}$ fullerenes.[7] These two cages are pretty similar, as shown in Figure 2. Structure $C_s$(39663)-$C_{82}$ can be obtained from $C_s$(51365)-$C_{84}$ after a Stone−Wales isomerization of two bonds and subsequent $C_2$ extrusion (Figure S2, SI). It is not coincidence that both cages show a low number of pyracylene units (Figure 3), just four and two for $C_{82}$ and $C_{84}$, respectively. As reported very recently,[8] structures with a low

(1) (a) Chaur, M. N.; Melin, F.; Ortiz, A. L.; Echegoyen, L. *Angew. Chem., Int. Ed.* **2009**, *48*, 7514–7538. (b) Martín, N. *Chem. Commun.* **2006**, 2093–2104.
(2) (a) Campanera, J. M.; Bo, C.; Poblet, J. M. *Angew. Chem., Int. Ed.* **2005**, *44*, 7230–7233. (b) Valencia, R.; Rodriguez-Fortea, A.; Poblet, J. M. *Chem. Commun.* **2007**, 4161–4163.
(3) Popov, A.; Dunsch, L. *J. Am. Chem. Soc.* **2007**, *129*, 11835–11849.
(4) Dunsch, L.; Yang, S. *Small* **2007**, *3*, 1298–1320.
(5) (a) Bolskar, R. D. *Nanomedicine* **2008**, *3*, 201–213. (b) Caravan, P.; Ellison, J. J.; McMurry, T. J.; Lauffer, R. B. *Chem. Rev.* **1999**, *99*, 2293–2352. (c) Fatouros, P. P.; Corwin, F. D.; Chen, Z. J.; Broaddus, W. C.; Tatum, J. L.; Kettenmann, B.; Ge, Z.; Gibson, H. W.; Russ, J. L.; Leonard, A. P.; Duchamp, J. C.; Dorn, H. C. *Radiology* **2006**, *240*, 756–764. (d) Zhang, E. Y.; Shu, C. Y.; Feng, L.; Wang, C. R. *J. Phys. Chem. B* **2007**, *111*, 14223–14226.
(6) Chaur, M. N.; Melin, F.; Athans, A. J.; Elliott, B.; Walker, K.; Holloway, B. C.; Echegoyen, L. *Chem. Commun.* **2008**, 2665–2667.
(7) (a) Zuo, T.; Walker, K.; Olmstead, M. M.; Melin, F.; Holloway, B. C.; Echegoyen, L.; Dorn, H. C.; Chaur, M. N.; Chancellor, C. J.; Beavers, C. M.; Balch, A. L.; Athans, A. J. *Chem. Commun.* **2008**, 1067–1069. (b) Mercado, B. Q.; Beavers, C. M.; Olmstead, M. M.; Chaur, M. N.; Walker, K.; Holloway, B. C.; Echegoyen, L.; Balch, A. L. *J. Am. Chem. Soc.* **2008**, *130*, 7854.
(8) Rodriguez-Fortea, A.; Alegret, N.; Balch, A. L.; Poblet, J. M. *Nature Chem.*, **2010**, DOI: 10.1038/NCHEM.837.

DOI: 10.1021/jo101620b Published on Web 11/08/2010

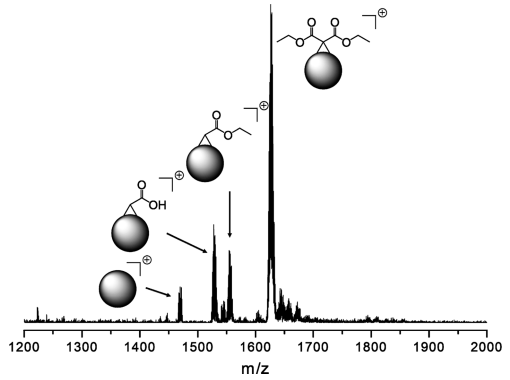


**FIGURE 1.** MALDI-TOF mass spectrum of the reaction mixture of $Gd_3N@C_{82}$, diethylbromomalonate and DBU in *o*-dichlorobenzene.

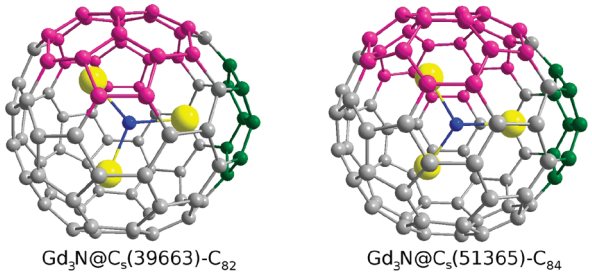


**FIGURE 2.** Representation of fullerenes $Gd_3N@C_{82}$ (left) and $Gd_3N@C_{84}$ (right). The adjacent pentagon pair is highlighted in green. The difference between the two structures is shown in pink.

number of pyracylene units are found among the most suitable cages to encapsulate metallic clusters. In particular, $C_s$(51365)-$C_{84}$ is the cage with the lowest number of pyracylenes among the 110 isomers with one adjacent pentagon pair (APP) and the 24 isomers that satisfy the IPR.

Here, we present a comprehensive computational study of the addition of methylbromomalonate on $Gd_3N@C_s$(39663)-$C_{82}$ and $Gd_3N@C_s$(51365)-$C_{84}$. Since calculations with metals that have unfilled 4f shells such as $Gd^{3+}$ ion ($f^7$) are not yet routine, the model that replaces $Gd^{3+}$ with $Y^{3+}$ is used. Such an approximation has been proposed earlier for modeling properties of $M_3N@C_{2n}$ (M = lanthanide).[9] Moreover, instead of ethylmalonate we used the methylmalonate as computational model. Initially, we analyzed the possibility of rotation of the cluster inside the carbon cage. Due to the egg-shaped framework of the $C_s$(51365)-$C_{84}$ and $C_s$(39663)-$C_{82}$ cages, the cluster is able to rotate only around the axis N−Y-centroid of the [5,5] bond, called from now on the "y axis". Only 2 kcal $mol^{-1}$ are necessary to rotate the cluster 45° around the *y* axis in the $Y_3N@C_{84}$, and 4 kcal $mol^{-1}$ to rotate 90° in the $Y_3N@C_{82}$ (see SI). One important difference between the two cages is that the $Y_3N$ cluster is able to freely rotate around the *y* axis in $C_s$(39663)-$C_{82}$, but rotation around this axis is hindered in $C_s$(51365)-$C_{84}$ (the energy increases by up to 23 kcal $mol^{-1}$ when the cluster rotates 90°) because it is more flattened than $C_{82}$. Moreover, the cluster does not fit well in any of the two egg-shaped cages when it is rotated around the other two perpendicular axes (see SI), so rotation around them is not feasible.

(9) (a) Popov, A. A. *J. Comput. Theor. Nanosci.* **2009**, *6*, 292–317. (b) Valencia, R.; Rodriguez-Fortea, A.; Clotet, A.; de Graaf, C.; Chaur, M. N.; Echegoyen, L.; Poblet, J. M. *Chem.—Eur. J.* **2009**, *15*, 10997–11009.

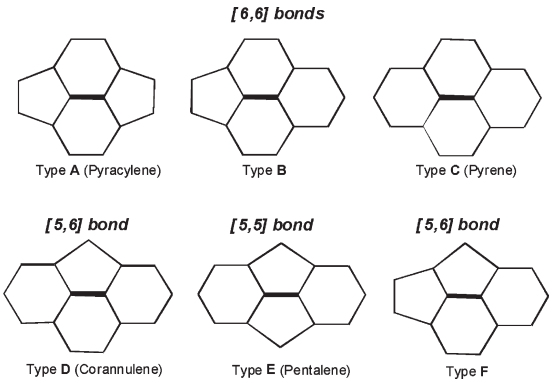


**FIGURE 3.** Different C−C bond types in the $C_s$(39663)-$C_{82}$ and $C_s$(51365)-$C_{84}$ cages.

**TABLE 1. Reaction Stabilities for the Different Computed Monoadducts and Most Significant Structural Parameters of Pristine $Y_3N@C_{84}$ and $Y_3N@C_{82}$**

| bond[a] | bond type | $d_{c-c}$[b] | $\theta_{pyr}$[c] | $\Delta E$[d] |
|---|---|---|---|---|
| | | $Y_3N@C_s$(51365)-$C_{84}$ | | |
| 78−82 | [5,5]-E | 1.449 | 12.55 | 9.0 |
| 22−23 | [5,6]-D | 1.461 | 12.85 | 9.4 |
| 77−84 | [5,6]-D | 1.461 | 11.28 | 0.0 |
| 79−80 | [5,6]-D | 1.463 | 11.40 | 7.5 |
| 80−81 | [5,6]-D | 1.458 | 11.34 | 4.4 |
| 83−84 | [5,6]-D | 1.464 | 11.26 | 0.2 |
| 23−24 | [6,6]-B | 1.472 | 11.37 | 4.5 |
| 32−33 | [6,6]-B | 1.468 | 12.30 | 4.7 |
| 24−45 | [6,6]-C | 1.485 | 8.75 | 7.6 |
| | | $Y_3N@C_s$(39663)-$C_{82}$ | | |
| 78−82 | [5,5]-E | 1.451 | 15.89 | 3.1 |
| 28−29 | [5,6]-D | 1.480 | 13.22 | 2.2 |
| 38−39 | [5,6]-D | 1.459 | 11.39 | 0.0 |
| 74−75 | [5,6]-D | 1.461 | 11.69 | 1.6 |
| 75−77 | [5,6]-D | 1.461 | 11.75 | 0.5 |
| 79−80 | [5,6]-D | 1.459 | 10.97 | 2.8 |
| 80−81 | [5,6]-D | 1.459 | 10.98 | 4.0 |
| 28−49 | [6,6]-B | 1.465 | 11.75 | 3.7 |
| 29−30 | [6,6]-B | 1.466 | 11.32 | 2.2 |

[a]The bond with which the malonate reacts. All the regioisomers shown here are open fulleroids. [b]Distance between the C atoms of the bond before the reaction takes place (in Å). [c]Average pyramidalization angle of the C atoms of the reacting bond (in degrees). [d]Relative energy (in kcal $mol^{-1}$) with respect to the lowest-energy regioisomer.

Table 1 shows the structural parameters of the principal C−C bonds in $Y_3N@C_{84}$ and $Y_3N@C_{82}$, for which we have computed the Bingel−Hirsch reaction along with the relative reaction energies of the resulting monoadducts. The reaction energies for all the analyzed bonds can be found in the SI. The labels of the C atoms as well as the bond type for each of the C−C bonds are also displayed (see Schlegel diagram in Figures 4 and 5). In addition to the [5,5] bond, there are different types of [5,6] and [6,6] bonds that are designated using the usual notation (see Figure 3).

As a general conclusion, we find that the most stable adducts form on C−C bonds whose distance is larger than the average C−C distance and whose pyramidalization angle is larger than the average angle. Accordingly, short C−C distances and small pyramidalization angles are related to unstable adducts. This dependence can be nicely observed when the relative energy of the different monoadducts is plotted against these two variables (see Figures 4 and 5). There is a region of low energy for large C−C distances and large pyramidalization angles. It is important to note that for

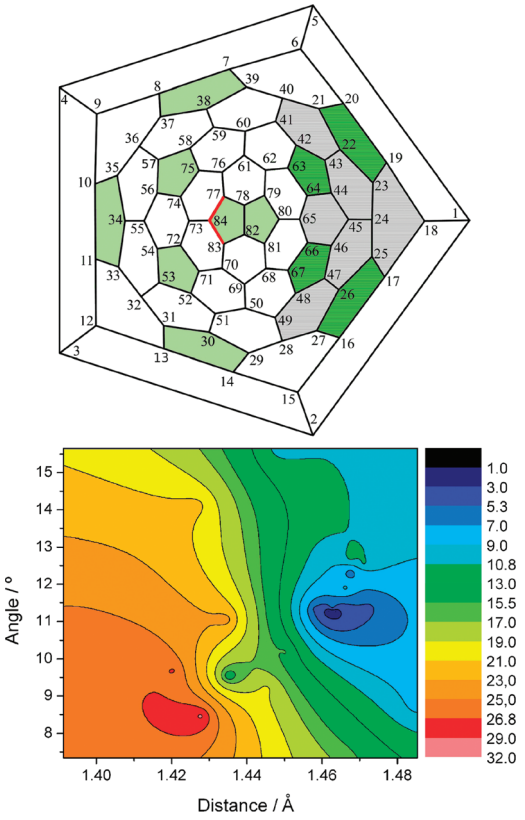


**FIGURE 4.** Schlegel diagram and two-dimensional (2D) plot of the relative energy (kcal mol$^{-1}$) of the computed monoadducts with respect to the C−C distances and the pyramidalization angles for $C_s$(51365)-$C_{84}$. The most reactive bonds (red) and the difference with respect to $C_s$(39663)-$C_{82}$ (gray) are highlighted.

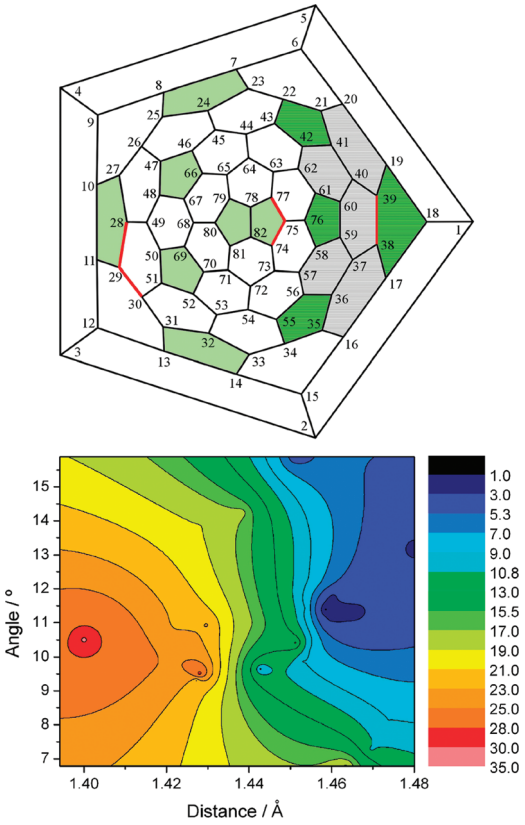


**FIGURE 5.** Schlegel diagram and 2D plot of the relative energy (kcal mol$^{-1}$) of the computed monoadducts with respect to the C−C distances and the pyramidalization angles for $C_s$(39663)-$C_{82}$. The most reactive bonds (red) and the difference with respect to $C_s$-(51365)-$C_{84}$ (gray) are highlighted.

most of the monoadducts (16 out of 21 for $Y_3N@C_{84}$ and 24 out of 29 for $Y_3N@C_{82}$), the C−C bond where the addition takes place is broken, as experimentally observed for $Y_3N@C_{80}$[10] and $Sc_3N@C_{68}$[11] and in contrast to what was found for $Sc_3N@C_{78}$.[12] The adducts with closed C−C bonds are within the most unstable structures. This bond breaking is mainly caused by the presence of the $M_3N$ cluster since most of the predicted adducts on the empty $C_{84}$ and $C_{82}$ cages feature closed C−C bonds (except for a few of them, see SI).

The origin of the stability of the adducts with large C−C distances and large pyramidalization angles can be the result of: (i) a topological effect, i.e. the type of C−C bond ([5,5], [5,6], etc.); or (ii) the presence of a nearby M atom from the encapsulated $M_3N$ cluster. Therefore, some bonds are intrinsically reactive as a consequence of the release of bond strain (as for example bond 77−84 in $Y_3N@C_{84}$ and 75−77 in $Y_3N@C_{82}$), whereas other bonds are activated by the presence of the $M_3N$ cluster (as for example bond 23−24 in $Y_3N@C_{84}$ and 38−39 in $Y_3N@C_{82}$; compare Tables 1 and S3, SI). There are five adducts of $Y_3N@C_{84}$ which show relative energies within 5 kcal mol$^{-1}$ (Table 1). The two most stable adducts correspond to the intrinsically reactive [5,6] bonds 77−84 and 83−84, see Figure 5. Nonetheless, the [5,5] bond 78−82 is not found to be among the most stable adducts (relative energy around 9 kcal mol$^{-1}$). Other bonds with longer C−C distances seem to give more stable adducts than the [5,5] bond.

On the other hand, for $Y_3N@C_{82}$, up to nine adducts show relative energies within 5 kcal mol$^{-1}$. The two most stable adducts correspond to one activated bond (38−39) and to one intrinsically reactive bond (75−77). The other low-energy adducts are also on intrinsically reactive (74−75) and activated bonds (28−29). The [5,5] 78−82 bond was found to be one of the most reactive bonds, but it does not lead to the most stable adduct (relative energy of around 3 kcal mol$^{-1}$). The [5,6]-D bonds with large C−C distances (75−77, 74−75, 79−80) result in more stable adducts than the [5,5] bond. Thus, the internal cluster clearly *activates* the 38−39 bond in $Y_3N@C_{82}$ that otherwise would yield a very unstable adduct (see Table S3, SI). However, the effect of the metal cluster is not so critical in $Y_3N@C_{84}$, the 77−84 bond being the most reactive (see Table S3, SI). It is worth noting that the intrinsically reactive bonds that give rise to the most stable adducts for the two non-IPR EMF considered here are bonds of [5,6]-D type that form part of the APP−pentalene unit (see Schlegel diagrams in Figures 4 and 5). Thus, the release of strain in the fullerene cages due to functionalization must be at the origin of such stable adducts.

Finally, we checked the validity of $Y_3N@C_{2n}$ as model for $Gd_3N@C_{2n}$. We computed a total of five adducts of different

(10) Lukoyanova, O.; Cardona, C. M.; Rivera, J.; Lugo-Morales, L. Z.; Chancellor, C. J.; Olmstead, M. M.; Rodriguez-Fortea, A.; Poblet, J. M.; Balch, A. L.; Echegoyen, L. *J. Am. Chem. Soc.* **2007**, *129*, 10423–10430.

(11) Cai, T.; Xu, L. S.; Shu, C. Y.; Reid, J. E.; Gibson, H. W.; Dorn, H. C. *J. Phys. Chem. C* **2008**, *112*, 19203–19208.

(12) Cai, T.; Xu, L.; Shu, C.; Champion, H. A.; Reid, J. E.; Anklin, C.; Anderson, M. R.; Gibson, H. W.; Dorn, H. C. *J. Am. Chem. Soc.* **2008**, *130*, 2136–2137.

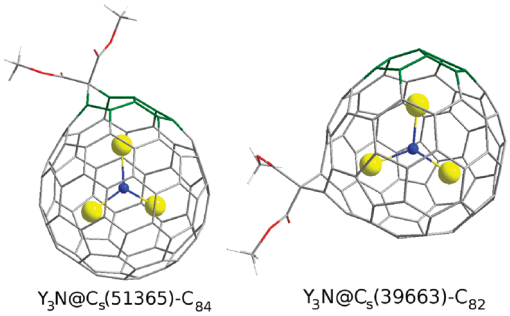


**FIGURE 6.** Representation of the most stable adducts in $Y_3N@C_{84}$ (bond 77−84, left) and $Y_3N@C_{82}$ (bond 38−39, right). The [5,5] bond is on top of the molecules (colored in green).

**TABLE 2. Relative Stabilities and Structural Parameters for Five Monoadducts of $Gd_3N@C_{84}$ and $Gd_3N@C_{82}$**

| bond[a] | bond type | $d_{c-c}$[b] | $\theta_{pyr}$[c] | $\Delta E$[d] |
|---|---|---|---|---|
| | | $Gd_3N@C_s(51365)$-$C_{84}$ | | |
| 77−84 | [5,6]-D | 1.462 | 11.28 | 0.0 |
| 83−84 | [5,6]-D | 1.464 | 11.26 | 0.1 |
| 23−24 | [6,6]-B | 1.472 | 11.37 | 3.2 |
| 32−33 | [6,6]-B | 1.468 | 12.30 | 3.7 |
| 78−82 | [5,5]-E | 1.449 | 15.65 | 10.0 |
| | | $Gd_3N@C_s(39663)$-$C_{82}$ | | |
| 38−39 | [5,6]-D | 1.459 | 11.46 | 0.0 |
| 75−77 | [5,6]-D | 1.461 | 11.81 | −0.2 |
| 29−30 | [6,6]-B | 1.466 | 11.32 | 1.3 |
| 78−82 | [5,5]-E | 1.452 | 15.88 | 4.3 |
| 75−76 | [6,6]-A | 1.401 | 10.52 | 32.4 |

[a]The bond with which the malonate reacts. All the regioisomers shown here are open fulleroids except 75−76. [b]Distance between the C atoms of the bond before the reaction takes place (in Å). [c]Average pyramidalization angle of the C atoms of the reacting bond (in degrees). [d]Relative energies (in kcal $mol^{-1}$) with respect to the lowest-energy regioisomer.

types for both fullerenes (the two most stable ones, adducts on activated bonds and on the [5,5] bond) (see Figure 6). The most important difference in the reaction energies with respect to the results obtained with our computational model $Y_3N@C_{2n}$ are, for $Gd_3N@C_{84}$ and the $Gd_3N@C_{82}$, only 1.5 kcal $mol^{-1}$ (for bond 23−24) and 1.6 kcal $mol^{-1}$ (for bond 29−30), respectively, which confirms the validity of present analysis. Computed values are displayed in Table 2.

Interestingly, for $Gd_3N@C_{82}$, the adduct on the [5,6]-D type 75−77 bond is somewhat more stable than the activated [5,6]-D type 38−39 bond. Since the energy differences between the most stable adducts are so small, the modeling by $Y_3N@C_{82}$ changes the relative stability of the two most stable isomers. The important point is, however, that the two most stable isomers show very similar energies.

To conclude, it is important to keep in mind that the rotation of the metal cluster around the N−Gd-centroid [5,5] bond in $Gd_3N@C_{82}$ can activate other bonds that would yield other adducts as stable as the ones that we have found. At the same time, bonds that are activated by the cluster (as for example 38−39) would become less reactive due to this internal rotation. On the other hand, other bonds, for example bond 75−77, will remain reactive regardless of the internal rotation. Thus, the prediction of the most abundant adduct (90%) of $Gd_3N@C_{82}$ is not a trivial task since a synergy between the addition process and the internal rotation of the cluster could exist. On the contrary, only two regioisomers are found to be the most stable when the Bingel−Hirsch reaction takes places on $Gd_3N@C_{84}$: adducts on bonds 77,84 and 83,84 (more than 3 kcal $mol^{-1}$ more stable than the other regioisomers). These two bonds, which are equivalent in the absence of the metal cluster, become equivalent due to the rotation of the $Gd_3N$ cluster around the *y* axis (up to 45°). Thus, our computations predict that only one regioisomer is much more stable than the rest in good agreement with experimental results.

To summarize, extension and rationalization of the reactivity of $Gd_3N@C_{2n}$ is reported in the present note. The functionalization of $Gd_3N$ non-IPR endohedral fullerenes via the Bingel−Hirsch reaction occurs in those bonds whose bond lengths and pyramidalization angles are larger than the average values. In particular, [5,6]-D bonds in the pentalene unit are found to yield the most stable adducts. Adducts on [6,6]-A bonds of pyracylene type, which are the most reactive in $C_{60}$, are not among the most stable regioisomers. In both EMFs analyzed here, rotation of the metal cluster around the N−M-centroid of the [5,5] bond axis is possible, which indicates that other activated bonds that we have not computed here may exist, especially for the $C_{82}$ cage. The small differences between the computed reaction energies for several monoadducts indicate that several different regioisomers are likely to coexist when the reaction occurs on $Gd_3N@C_{82}$, in good agreement with the experimental results that show the presence of three monoadducts (90%, 7%, and 3%). For $Gd_3N@C_{84}$, a single regioisomer is predicted, in agreement with experiments as well.

## Experimental Section

Samples of $Gd_3N@C_{2n}$ ($2n$ = 82 and 84) were synthesized and purified as described before.[6] The given MN EMF was dissolved in *o*-DCB under argon atmosphere, and then 20 equiv of bromodiethylmalonate was added. Finally 20 equiv of DBU was slowly added at room temperature. The progress of the reaction was followed by TLC, and the products were isolated by HPLC chromatography.

All the calculations were performed with the ADF2007 code,[13] and the Slater TZP quality basis set and by using BP86 functionals.[14] The carbon cages of $C_s$ symmetry have 67 ($C_{84}$) and 66 ($C_{82}$) different C−C bonds. The symmetry of the MN EMF is reduced to $C_1$ when the X-ray structure is considered (126 bonds for $C_{84}$ and 123 for $C_{82}$). In this study we have assumed a pseudo-$C_s$ symmetry for the EMF since the plane of the cluster is near the $\sigma_h$ plane that relates the two halves of the $C_{2n}$ cages.

**Acknowledgment.** Financial support from the NSF (Grant number DMR-0809129) is greatly appreciated. This work was also supported by the Spanish Ministry of Science and Innovation [CTQ2008-06549-C02-01/BQU and the RyC Program (ARF)] and by the Generalitat de Catalunya (2009SGR462 and XRQTC).

**Supporting Information Available:** HPLC trace of the mixture of $Gd_3N@C_{82}$-monoadducts; relative energies for different isomers of pristine EMFs; reaction energies and structural parameters for all the adducts; a figure that relates structures $C_s(39663)$-$C_{82}$ and $C_s(51365)$-$C_{84}$; and Cartesian *xyz* coordinates for the most representative adducts. This material is available free of charge via the Internet at http://pubs.acs.org.

(13) (a) *ADF 2007.01*; SCM, Department of Theoretical Chemistry, Vrije Universiteit: Amsterdam, 2007; http://www.scm.com. (b) te Velde, G. T.; Bickelhaupt, F. M.; Baerends, E. J.; Guerra, C. F.; Van Gisbergen, C. J. A.; Snijders, J. G.; Ziegler, T. *J. Comput. Chem.* **2001**, *22*, 931–967.

(14) (a) Becke, A. D. *Phys. Rev. A* **1988**, *38*, 3098–3100. (b) Perdew, J. P. *Phys. Rev. B* **1986**, *33*, 8822–8824.